TOXICOLOGICAL SCIENCES, 2018, 1–10

doi: 10.1093/toxsci/kfy120
Advance Access Publication Date: May 21, 2018
Research Article

Microvascular Dysfunction Following Multiwalled Carbon Nanotube Exposure Is Mediated by Thrombospondin-1 Receptor CD47

William Kyle Mandler,[*,†] Timothy R. Nurkiewicz,[†,‡,§] Dale W. Porter,[†,¶] Eric E. Kelley,[†,‡,§] and Ivan Mark Olfert[*,†,‡,§,1]

[*]Division of Exercise Physiology, West Virginia University School of Medicine, Morgantown, WV 26506; [†]Toxicology Working Group, West Virginia University School of Medicine, Morgantown, WV 26506; [‡]Department of Physiology, Pharmacology and Neuroscience, West Virginia University School of Medicine, Morgantown, WV 26506; [§]West Virginia Clinical and Translational Science Institute, Robert C. Byrd Health Sciences Center, Morgantown, WV 26506; and [¶]National Institute for Occupational Safety and Health, Morgantown, WV 26505

Disclaimer: The findings and conclusions in this report are of the authors and do not necessarily represent the views of the National Institute for Occupational Safety and Health and the mention of brand name products does not constitute product endorsement. Mention of product or company name constitutes neither endorsement nor rejection by the Centers for Disease Control and Prevention or NIOSH.

[1]To whom correspondence should be addressed at West Virginia University School of Medicine, One Medical Center Drive, PO Box 9227, Morgantown, WV 26506. Fax: (304) 293-7597. E-mail: imolfert@hsc.wvu.edu.

ABSTRACT

Pulmonary exposure to multiwalled carbon nanotubes (MWCNTs) disrupts peripheral microvascular function. Thrombospondin-1 (TSP-1) is highly expressed during lung injury and has been shown to alter microvascular reactivity. It is unclear exactly how TSP-1 exerts effects on vascular function, but we hypothesized that the TSP-1 receptor CD47 may mediate changes in vasodilation. Wildtype (WT) or CD47 knockout (CD47 KO) C57B6/J-background animals were exposed to 50 μg of MWCNT or saline control via pharyngeal aspiration. Twenty-four hours postexposure, intravital microscopy was performed to assess arteriolar dilation and venular leukocyte adhesion and rolling. To assess tissue redox status, electron paramagnetic resonance and NOx measurements were performed, while inflammatory biomarkers were measured via multiplex assay. Vasodilation was impaired in the WT + MWCNT group compared with control (57 ± 9 vs 90 ± 2% relaxation), while CD47 KO animals showed no impairment (108 ± 8% relaxation). Venular leukocyte adhesion and rolling increased by >2-fold, while the CD47 KO group showed no change. Application of the antioxidant apocynin rescued normal leukocyte activity in the WT + MWCNT group. Lung and plasma NOx were reduced in the WT + MWCNT group by 47% and 32%, respectively, while the CD47 KO groups were unchanged from control. Some inflammatory cytokines were increased in the CD47 + MWCNT group only. In conclusion, TSP-1 is an important ligand mediating MWCNT-induced microvascular dysfunction, and CD47 is a component of this dysregulation. CD47 activation likely disrupts nitric oxide (•NO) signaling and promotes leukocyte-endothelial interactions. Impaired •NO production, signaling, and bioavailability is linked to a variety of cardiovascular diseases in which TSP-1/CD47 may play an important role.

Key words: endothelial dysfunction; pulmonary exposure; nanomaterials.

Engineered nanomaterials (ENMs) are rapidly becoming an integral component of modern composite material manufacturing. Nanomaterials may be comprised of a wide range of chemical compositions and molecular structures, but by definition they must possess at least 1 dimension < 100 nm. This scale provides advantages for manufacturing but nanomaterials are also more

readily aerosolized and deposited into the deep lung upon inhalation, making them more dangerous than the same materials of larger particle size (Bakand *et al.*, 2012). Of particular concern is a class of ENM, multiwalled carbon nanotubes (MWNCTs). Although heterogeneous in physicochemical properties (eg, aspect ratio, metal contamination, attached functional groups) all MWCNT are comprised of layers of graphene arranged in concentric tubes. Pulmonary symptoms of exposure to most MWCNT species include increased neutrophil influx, genotoxicity, lymphocytic aggregates, and fibrosis (Mercer *et al.*, 2011).

There is evidence that in addition to direct damage to pulmonary tissue, exposure to nanomaterials is capable of generating deleterious systemic effects. The antivasodilatory effect for this route of exposure in arterioles has been previously established (LeBlanc *et al.*, 2009; Nurkiewicz *et al.*, 2009). Arterioles play a critical role in contributing to the maintenance of homeostasis. Impaired control of arteriolar diameter, especially the ability to dilate appropriately, has been associated with a variety of serious disease states, including hypertension (Perticone *et al.*, 2001; Petrak *et al.*, 2006), peripheral/coronary artery disease (Brevetti *et al.*, 2008; Heitzer *et al.*, 2001), and atherosclerosis (Bonetti *et al.*, 2003; Davignon and Ganz, 2004; Sitia *et al.*, 2010). Pulmonary MWCNT exposure has been linked to each of the above conditions (Aragon *et al.*, 2016; Cao *et al.*, 2014; Han, 2016; Stapleton *et al.*, 2012; Thompson *et al.*, 2014). Our group has previously established that an exceedingly small fraction (<0.03%) of total MWCNT lung burden escapes the lung and is deposited in the peripheral tissues (Mercer *et al.*, 2013b). Because such a small proportion of MWCNT escape the lung to directly interact with extrapleural tissues, it is likely that some intermediate factors may be responsible for peripheral effects.

The molecular mechanisms linking pulmonary MWCNT exposure to microvascular dysfunction have yet to be fully elucidated. Among several putative pathways, one is that innate immune responses can trigger release of vasoactive factors that act systemically. Acute lung injury and inflammation promotes macrophage influx, leukocyte adhesion (Inoue *et al.*, 2009), and the formation of leukocyte-platelet aggregates (Zarbock and Ley, 2009). The matricellular matrix protein thrombospondin-1 (TSP-1) is a major component of the α-granules of platelets, and is released upon platelet activation (Baenzige *et al.*, 1971). We have recently demonstrated that pulmonary exposure to MWCNT resulted in increased peripheral TSP-1 protein in wild-type (WT) C57BL/6 J background mice, along with reduced arteriolar dilatory capacity, and increased leukocyte venular adhesion and rolling (Mandler *et al.*, 2017). TSP-1 knockout (KO) mice exposed to MWCNT were protected from the negative changes in arteriolar reactivity experienced by WT control animals. Elevated TSP-1 expression and impaired vascular function following MWCNT exposure have also recently been observed by another group (Aragon *et al.*, 2016, 2017).

TSP-1 is capable of influencing vessel diameter via several pathways. In particular, TSP-1 inhibits nitric oxide (NO) and Cyclic guanosine monophosphatee (cGMP) signaling through the cell surface receptor CD47, which inhibits soluble guanylate cyclase (sGC) (Isenberg *et al.*, 2005). At picomolar concentrations, TSP-1 is capable of completely inhibiting NO-stimulated production of cGMP by sGC, thus limiting vascular smooth muscle relaxation (Isenberg *et al.*, 2006). CD47 signaling is also capable of causing endothelial Nitric Oxide Synthase uncoupling and generation of ROS (Bauer *et al.*, 2012). In addition to directly inhibiting NO signaling and production, it is also possible that TSP-1 may indirectly influence arteriolar diameter by promoting the recruitment of leukocytes to the endothelium through activation of intracellular and vascular adhesion molecules (ICAM-1, VCAM-1) (Narizhneva *et al.*, 2005). As these activated leukocytes adhere, roll, flatten, and undergo transendothelial migration, production of superoxide ($O_2^{\bullet -}$) by NADPH oxidase can quench NO as it is produced, reducing its bioavailability (Hopps *et al.*, 2009). Superoxide is rapidly converted to H_2O_2 by superoxide dismutase (SOD), and may exert effects on vascular reactivity independent of NO (Bauer *et al.*, 2012; Knuckles *et al.*, 2013). Local oxidative and nitrositive stress are hallmarks of leukocyte endothelial interactions (Kar and Kavdia, 2012).

Although the evidence for the role of TSP-1 as a key mediator in the pathophysiology of microvasculature dysfunction following nanomaterial exposure is strong, the relative contribution of various pathways has yet to be determined. Additionally, the upstream signals of TSP-1 in the lung, circulation, and skeletal muscle in this context are unclear. The objective of the current work is to determine the role of CD47 in following pulmonary MWCNT exposure, identify potential inflammatory regulators of TSP-1, and measure changes in the redox status lung, blood, and skeletal muscle. We hypothesize that CD47 is a critical receptor for TSP-1 mediated alterations in vascular function following pulmonary MWCNT exposure, and as such, CD47 KO animals will be afforded some degree of protection from the vascular consequences of this exposure.

METHODS AND MATERIALS

Animals. C57BL/6 J background *Cd47*^{tm1Fpl} (CD47 KO) and WT were purchased from Jackson Labs, Bar Harbor, ME (Stock No. 003173 and 000664, respectively) and assigned to either sham or MWCNT aspiration exposure groups (described below). Mice were handled according to NIH Use of Laboratory Animals, Animal Welfare Act, and all experiments were approved by the West Virginia University Institutional Animal Care and Use Committee. Mice were kept on a 12-h light/dark cycle, and provided food and tap water ad libitum. Experiments were scheduled so that data collection occurred at approximately 16 weeks of age. At this age, the mice are sexually and developmentally mature and the gluteus maximus muscle is of sufficient size and strength to undergo intravital microscopy (Flurkey *et al.*, 2007). Both male and female WT and KO animals were used in all experiments in approximately equal numbers (Table 1).

Nanomaterial exposure details. MWCNT are catalytically grown by chemical vapor deposition processes and were obtained from Mitsui & Co (MWNT-7, Lot No. 061220-31, Ibaraki, Japan). Mitsui-7 MWCNTs were designated as the ENM of choice for this project based on the wide number of potential applications, observed toxicity, and prior investigations by our group (Mandler *et al.*, 2017; Porter *et al.*, 2010). When dispersed in the manner in this paper, the mean length is 3.86 ± 1.94 μm and width of 49 ± 13.4 nm (Porter *et al.*, 2010). Oropharyngeal aspiration, as opposed to intratracheal instillation or aerosol inhalation was chosen as the method of exposure for this study due to the high degree of flexibility and scalability compared with inhalation. Prior studies have shown that aspiration of this (50 μg/mouse) and similar doses of MWCNT in dispersion medium (DM) generates pulmonary response analogous to instillation (Bonner *et al.*, 2013) and inhalation (Mercer *et al.*, 2011; Shvedova *et al.*, 2008).

In brief, prior to aspiration, 50 μg MWCNT is suspended and dispersed in a phospho-buffered saline/purified mouse serum albumin medium using ultrasonication. Although anesthetized (isoflurane), the solution is placed in the oropharynx with the tongue manually extended and the animal was restrained until it

Table 1. Animal Characteristics

Animal Characteristics				
	WT + SHAM	WT + MWCNT	CD47 KO + SHAM	CD47 KO + MWCT
n Mice (male:female)	14 (7:7)	15 (7:8)	4 (2:2)	6 (3:3)
Age (weeks)	16.5 ± 0.6	16.4 ± 0.5	15.8 ± 0.0	16.1 ± 0.2
Bodyweight (g)	26.5 ± 0.8	25.1 ± 0.8	24.9 ± 1.2	24.8 ± 0.9

No significant differences were observed between groups in age, weight, or sex.

took 2 full breaths. This dose and delivery method has previously been shown to induce lung injury and inflammation (Porter *et al.*, 2010). The 50 μg exposure level is approximately equivalent to a human performing light work for 5 months in an environment with MWCNT aerosol of 400 $\mu g/m^3$ (Porter *et al.*, 2010). This particle concentration (430 $\mu g/m^3$) has been observed in a laboratory studying MWCNT (Han *et al.*, 2008). Control animals received a sham aspiration of DM without nanomaterials. This DM has been shown to be both biocompatible, nonimmunogenic, and effective at dispersing MWCNT (Porter *et al.*, 2008, 2010).

Intravital microscopy and iontophoresis of mouse gluteus maximus arterioles. At 24-h postaspiration, KO or WT mice were anesthetized using thiobutabarbital (Inactin, 100 mg/kg, i.p.) and placed on a thermo-probe regulated heating pad to maintain a 37°C core temperature. The trachea was intubated to ensure a patient airway. The right gluteus maximus muscle was surgically exteriorized for microscopic observation, leaving its innervation and all feed vessels intact. This site of observation was chosen as skeletal muscle is the largest global reservoir of the microvasculature and the largest source of active peripheral resistance. After exteriorization, the muscle was secured over an optical pedestal with 5-0 suture wire at its *in situ* length. The pedestal was sealed with stopcock grease to create a superfusate bath. Throughout the surgery and following experimental period, the muscle was continuously superfused with a physiologic saline solution (PSS) (119 mM NaCl, 25 mM $NaHCO_3$, 6 mM KCl, and 3.6 mM $CaCl_2$), warmed to 35°C, and equilibrated with 95% N_2 –5% CO_2 (pH = 7.35–7.40). Superfusate flow rate was maintained at 4 ml/min to minimize equilibration with atmospheric oxygen.

The animals were transferred to an intravital microscope coupled to a digital video camera. Observations were made with a 20× water immersion objective. A micropipette with an opening of 1–2 μm was filled with a 10^{-2} M acetylcholine (to measure endothelium-dependent vasodilation) solutions. The tip of the pipette was guided under microscope to a point adjacent to the adventitia of the target arteriole. During this time a holding current of −200 or 200 nA, respectively, was applied to the bath to prevent ACh/SNP leakage from the pipette. Once in place and following a 20-min equilibration period, ejection currents of 20, 40, and 80, and 120 nA (for ACh) were applied to the bath for 5 min each in a randomized order, with a 5-min washout period between each step. Following the final ACh washout period, adenosine was added to the superfusate at a concentration of 10^{-3} M to determine vessel maximal passive diameter. Images were displayed on a high-resolution computer monitor and digitally captured in the last minute of each step for later analysis using ImageJ (ImageJ 1.46v, National Institutes of Health). One to three first order arterioles were studied per mouse. Measurements of vessel diameter were made from recorded images. Vessel reactivity is reported as percent of maximal diameter achieved. Resting vascular tone was calculated for each vessel as follows:

$$\text{tone} = \left[\frac{\text{Dpass} - \text{Dc}}{\text{Dpass}}\right] \times 100,$$

where D is arteriolar diameter, in micrometers, and D_{pass} is passive diameter under ADO, and D_c is the diameter measured during the control period. D_c was taken following a 20-min equilibration and only if no change in vessel diameter had been observed for at least 1 min prior. Percent relaxation was calculated at each ACh or SNP ejection current as follows:

$$\%\ \text{relaxation} = \left[\frac{\text{Dpass} - \text{Dion}}{\text{Dpass} - \text{Dc}}\right] \times 100,$$ where D_{ion} is the vessel diameter following 5 min of drug delivery via iontophoresis. The number of animals and arterioles studied can be found in Tables 1 and 2.

Leukocyte adhesion and rolling. Leukocytes that were either stationary or moving but in constant contact with the venular wall for at least 200 μm were counted for 1 min in each venule studied. Following the completion of iontophoresis studies and after a 20-min washout period, 10^{-4} M apocynin was added to the superfusate to examine contributions of reactive oxygen species. Following a 30-min apocynin incubation period, the measurements were repeated during apocynin superfusion. Number of venules studied for each group is as follows: WT + SHAM (n = 13), WT + MWCNT (n = 13), CD47 KO + MWCNT (n = 8). CD47 KO + SHAM (n = 6).

Tissue redox status. At the conclusion of intravital experiments, 100 μl of whole blood was collected from each experimental animal and incubated with the electron paramagnetic resonance (EPR) spin probe 4-phosphonooxy-2, 2, 6, 6-tetramethylpiperidine-N-hydroxyl (PPH) for 10 min at a final concentration of 0.25 mM before being snap frozen for later analysis. EPR was used to detect superoxide ($O_2^{\bullet -}$) and in biologic samples, spectra were obtained using a Bruker EMX EPR spectrometer equipped with a Bruker ER4119 HS resonator. Samples were prepared in 1.5 ml plastic centrifuge tubes and were transferred to a quartz flat cell (Wilmad Glass Co, Buena, New Jersey) before spectra were obtained. Superoxide levels were estimated from the magnitude of the downfield peak height of the 3-line nitrogen hyperfine as well as the area under the curve and were expressed in arbitrary units. Validation of $O_2^{\bullet -}$ was accomplished by ablation of the signal in the presence of SOD.

$^{\bullet}NO$ has an extremely short half-life *in vivo* and is rapidly converted to intermediates. Tissue NO_x (nitrate + nitrite) was measured by first chemically reducing NO_x to $^{\bullet}NO$ gas (0.05 M vanadium chloride [VCl_3] in 1 M HCl at 92°C) as described by (Braman and Hendrix, 1989) and then detecting the light generated by reaction of $^{\bullet}NO$ gas with O_3 using a Sievers 280i $^{\bullet}NO$ analyzer (NOA) (Boulder, Colorado). A 50-ml glass impinger vial containing 30-ml VCl_3 (0.4 M in 1 M HCl) at 95°C. Nitrogen gas

Table 2. Baseline Vessel Characteristics

Arteriole Characteristics				
	WT + SHAM	WT + MWCNT	CD47 KO + SHAM	CD47 KO + MWCT
n (vessels)	21	15	8	8
Baseline diameter (μm)	34.4 ± 2.4	34.9 ± 2.0	30.6 ± 3.1	34.4 ± 2.8
Passive diameter (μm)	52.0 ± 2.6	49.6 ± 2.6	51.1 ± 2.6	47.5 ± 3.5
Resting tone (%)	32.2 ± 2.8	26.1 ± 4.1	39.9 ± 5.3	27.5 ± 3.2

No significant differences were observed between exposure groups of vessels used for microiontophoresis experiments in baseline or passive diameter, or resting tone.

was bubbled through the water trap containing 10 ml NaOH, and delivered to the NOA. A standard curve was generated (Liquid Program software v 3.22 PNN, Sievers) and used to calculate •NO released by each injected sample. Samples (25 μl) were run in duplicate and chemiluminescence analyzed by the NOA. Number of animals studied: WT + SHAM (n = 14), WT + MWCNT (n = 5), CD47 KO + MWCNT (n = 6).

Tissue inflammatory markers. Inflammatory cytokines (Interleukin [IL]-6, IL1-β, IL-10, Vascular Endothelial Growth Factor [VEGF], Tumor Growth Factor [TGF]-β, and TNF-α) were quantified by U-Plex Meso Scale Discovery multi-cytokine array (Meso Scale Diagnostics, Gaithersburg, Maryland), according to manufacture instructions, in the lung, plasma, and gluteus maximus. Experiments were performed in duplicate for each animal. Number of animals studied: WT + SHAM (n = 14), WT + MWCNT (n = 5), CD47 KO + MWCNT (n = 6).

Statistics and calculations. A D'Agostino and Pearson omnibus normality test was used to assess homogeneity of variance. In cases where non-normal datasets were detected, statistical comparisons were made with Kruskal–Wallis tests and post hoc Wilcoxon rank-sum tests for between subject effects where appropriate. A 2 × 2 factorial ANOVA was performed to compare the main effects of exposure (sham vs MWCNT) and genotype (WT vs KO) for each variable. When significant main effects were observed a Sidak post hoc test was used to determine where significant differences existed between the groups. In all cases, $p < .05$ was used to establish statistical significance. All data are reported as mean ± SEM, unless otherwise noted.

RESULTS

No differences were observed between groups in age or weight (Table 1). Ratios of male to female animals used were equal or very close to equal. Arterioles examined in this study averaged approximately 34.5 μm in diameter across all groups (Table 2). No differences between treatment groups were observed in baseline diameter, passive diameter, or resting tone (Table 2). There were also no significant sex differences in vessel baseline diameter, maximal passive diameter, or reactivity before and after nanomaterial exposure.

Arteriolar Endothelium Dependent Reactivity

Arteriolar endothelium dependent reactivity was measured via intravital microscopy. ACh administration yielded a dose-dependent increase in WT + SHAM arterioles, reaching 89.6% of passive diameter at the highest ACh ejection current (Figure 1) . The WT + MWCNT arterioles demonstrated impaired vasodilation at 40, 80 and 120 nA ACh, achieving only 56.8% of passive diameter, an impairment of 32.8% compared with controls (Figure 1). Vessels in CD47 KO animals exposed to MWCNT displayed no impaired ACh response, and even exceeded the control group at the 80 nA level achieving 105.3% of passive diameter (Figure 1).

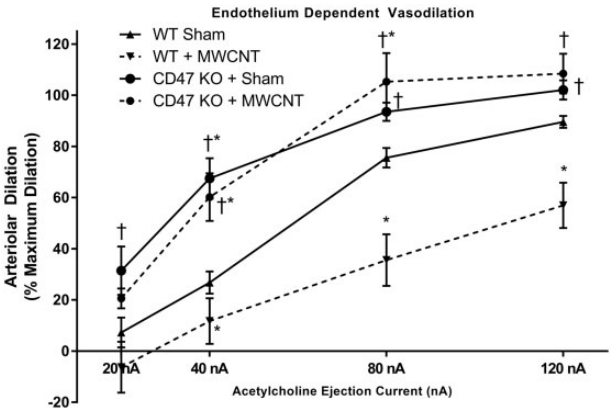

Figure 1. Endothelium dependent vasodilation in gluteus maximus arterioles. Arteriolar dilation presented as percent of maximal passive dilation achieved with adenosine. Asterisk indicates difference ($p < .05$) from WT + Sham group. Dagger indicates difference from WT + MWCNT group ($p < .05$). Number of arterioles studied for each group is as follows: WT + SHAM (n = 21), WT + MWCNT (n = 15), CD47 KO + MWCNT (n = 8), CD47 KO + SHAM (n = 8).

Venular Leukocyte Adhesion and Rolling

The flux of leukocytes through target venules was assessed at baseline and following application of antioxidant/ NADPH oxidase-1(NOX1) inhibitor apocynin. MWCNT exposure increased leukocyte flux by 222% compared with WT control (Figure 2). MWCNT exposure elicited no significant increase in leukocyte flux in the CD47 KO group. Application of apocynin rescued normal leukocyte flux in the WT + MWCNT group and depressed values in the other groups (Figure 2). Given that CD47 KO sham and CD47 KO MWCNT-exposed mice exhibited no differences in vascular reactivity or leukocyte adhesion and rolling, mediators of these responses were not investigated in this group.

Tissue Redox Status

No differences between any groups were observed in $O_2^{\bullet -}$ content in whole blood using EPR with the spin probe agent PPH (Figure 3). Tissue NOx was assessed using a Sievers NOA. In the Lung, NOx was reduced by 47% in WT + MWCNT animals, compared with control, while NOx levels in CD47 KO + MWCNT animals were not different from controls (Figure 4). A similar pattern was observed in the plasma, with a 32.3% NOx reduction in WT + MWCNT animals and no change in the CD47 KO + MWCNT group.

Tissue Inflammatory Markers

No differences in any measure were observed between WT groups; however, several markers were different from control

compared with the CD47KO + MWCNT group. In the lung, IL-6 was elevated and VEGF was depressed in CD47 + MWCNT animals. In the plasma, IL-6, IL-10, VEGF, and TNF-α were all elevated in CD47 KO + MWCNT animals compared with control and WT + MWCNT groups. In gluteus muscle tissue, VEGF was depressed, while TNF-α was enhanced in CD47 + MWCNT animals. No differences between any groups were observed in measures of TGF-β or IL1-β.

DISCUSSION

The principal finding of this study is that the CD47 receptor plays a critical role in the vascular dysfunction associated with lung exposure to MWCNT. We observed that CD47KO + MWCNT animals exhibited similar, or even greater, levels of arteriolar endothelium-dependent vasodilation in response to ACh stimulation than WT + SHAM controls. TSP-1 normally circulates at a low (0.22 nM), but vasoactive concentration (Csanyi *et al.*, 2012) acting as a limiting factor to NO signaling. Removal of this "brake" influence through ablation of this signaling pathway enhances responsiveness to vasodilatory stimuli. These findings closely resemble patterns of dilation achieved by TSP-1 KO animals in our previous work (Mandler *et al.*, 2017), as well as arterioles from CD47 KO and TSP-1 KO animals observed in other intravital microscopy experiments (Bauer *et al.*, 2010). When exposed to MWCNT, CD47 KO animals exhibited no decrease in dilatory capacity compared with WT animals (where relaxation was impaired by approximately 33%). The protection offered by CD47 KO strongly suggests that CD47 is integral in mediating impairments following pulmonary MWCNT exposure.

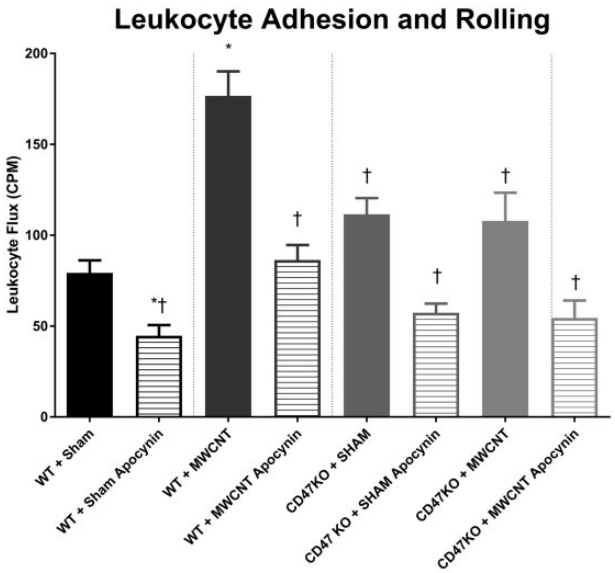

Figure 2. Venular leukocyte adhesion and rolling activity. Asterisk indicates difference from WT + SHAM with PSS ($p < .05$). Dagger indicates difference from WT + MWCNT with PSS ($p < .05$). Number of venules studied for each group is as follows: WT + SHAM ($n = 13$), WT + MWCNT ($n = 13$), CD47 KO + MWCNT ($n = 8$). CD47 KO + SHAM ($n = 6$).

The relevance of bolus dosing by oropharyngeal aspiration in comparison to whole body inhalation continues to be an area of debate. In regards to MWCNT, our laboratory has demonstrated that MWCNT distribution, as well as acute inflammation, is similar for both methods of exposure. In regards to distribution, 1 day after pharyngeal aspiration exposure, 81.6% and 18% of the MWCNT lung burden was in the alveolar and airway compartments, respectively (Mercer *et al.*, 2010). For mice exposed to MWCNT by whole body inhalation, 1 day after exposure were completed, had 84% and 16% of the MWCNT lung burden was in the alveolar and airway compartments, respectively (Mercer *et al.*, 2013a). Thus, oropharyngeal aspiration and whole body inhalation resulted in similar MWCNT distributions in the lung. In regards to acute inflammatory response, comparison of whole lung lavage PMNs demonstrated the responses to 10 μg MWCNT by oropharyngeal aspiration was similar to whole body inhalation dose of 13 μg MWCNT (Porter *et al.*, 2012).

One mechanism through which MWCNT exposure ultimately exerts its effects on peripheral microvasculature presumably involves impairment of $^{\bullet}NO$ generation, signaling, and/or bioavailability. Although we did not detect any changes in $O_2^{\bullet -}$ levels using EPR (perhaps due to the abundance of heme, biomolecular-bound iron and protein in blood), we observed that NO is depressed in lung and plasma following MWCNT, and that CD47 KO animals are protected from this effect. Our

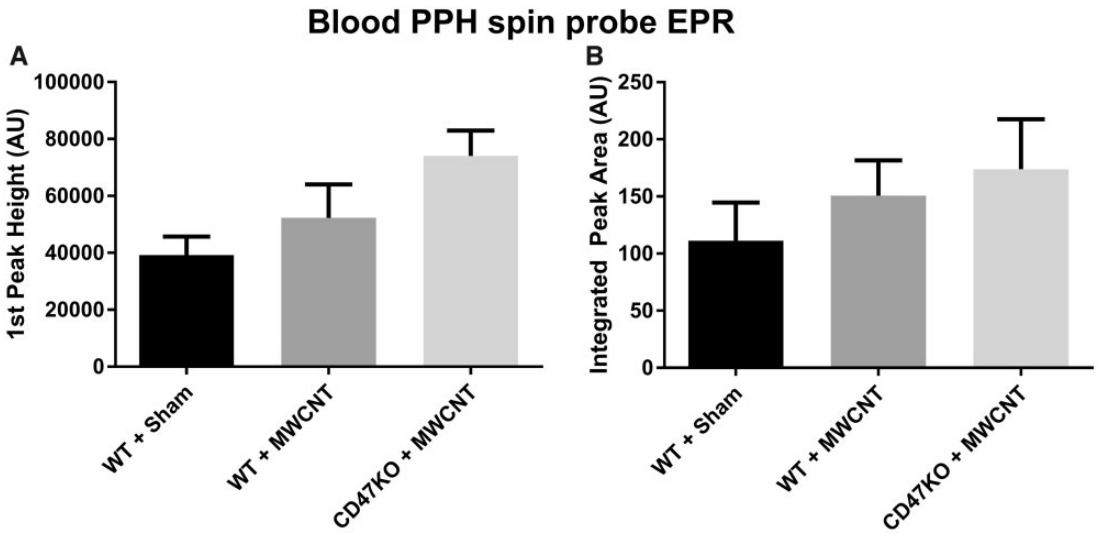

Figure 3. Blood superoxide content. No differences between groups were observed in either first peak height (A) or integrated peak area (B) in blood samples using EPR with the spin trap compound PPH. Number of animals studied: WT + SHAM ($n = 14$), WT + MWCNT ($n = 5$), CD47 KO + ($n = 6$).

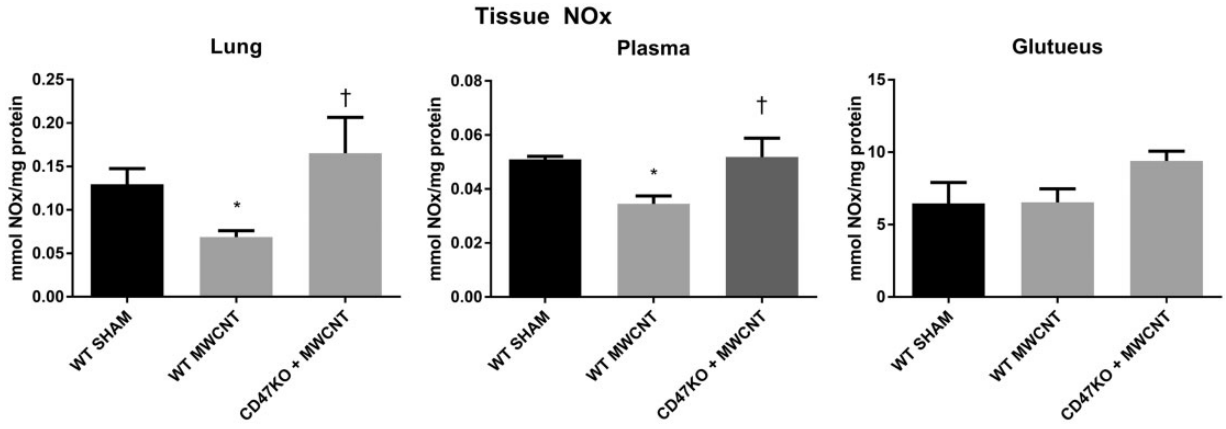

Figure 4. Tissue NOx. NOx was reduced in WT + MWCNT lung and plasma samples, compared with WT + SHAM (*) ($p < .05$). NOx was elevated compared with WT + MWCNT in CD47KO + MWCNT lung and plasma (†) ($p < .05$) No differences in between any groups were observed in the gluteus maximus tissues. Number of animals studied: WT + SHAM ($n = 14$), WT + MWCNT ($n = 5$), CD47 KO + MWCNT ($n = 6$).

leukocyte adhesion analysis may also yield some additional information on vessel ROS status. CD47 signaling is capable of activating NOX1 in, both, the endothelium (Csanyi *et al.*, 2012) and circulating leukocytes (Barclay, 2009). Generating ROS promotes leukocyte adhesion through P-selectin mobilization (Granger and Senchenkova, 2010). CD47 signaling also promotes leukocyte adhesion through ICAM-1/VCAM-1 activation (Lagadec *et al.*, 2003; Narizhneva *et al.*, 2005), which in turn activates NOX1 within minutes (Deem and Cook, 2004), and promotes endothelial disorganization and permeability (DelMaschio *et al.*, 1996). CD47 KO animals have reduced leukocyte recruitment into dermal air pouches, and reduced transmigration even when stimulated with TNF-α (Azcutia *et al.*, 2012). In this study, CD47 KO animals did not exhibit increased leukocyte flux following MWCNT exposure (compared with WT animals), and application of apocynin (an antioxidant/NOX1 inhibitor) rescued normal leukocyte flux in the WT + MWCNT group, and reduced levels to below PSS alone in WT + SHAM and CD47 KO + MWCNT groups. Pulmonary nanoparticle exposure generates oxidative and nitrositive stress in the microvascular wall (LeBlanc *et al.*, 2010; Nurkiewicz *et al.*, 2009), our findings suggest that TSP-1/CD47 signaling contribute to this effect and promote endothelial cell adhesion and transmigration, which can further exacerbate endothelial dysfunction.

Aragon *et al.* (2016, 2017) have recently investigated the contributions of another TSP-1 receptor, CD36, to MWCNT-exposure induced vascular dysfunction. The authors observed that isolated aortic rings in CD36 KO mice did not exhibit significant reductions in vasodilation reactivity following incubation in serum collected from MWCNT-exposed mice, despite increase in circulating TSP-1 protein. In contrast, similar to our data, aorta reactivity in WT mice were dramatically impaired at 4 and 24-h postexposure. In WT aortas incubated in serum from matrix metalloproteinase-9 (MMP-9) KO animals exposed to MWCNT, no significant impairment was also noted, suggesting involvement of MMP-9/TSP-1/CD36 signaling axis. More investigation is necessary to reconcile the findings of Aragon *et al.* with our work with TSP-1 and CD47 KO animals. It is possible that ablation of a single TSP-1 signaling axis is sufficient to offer protection. It is important to note, however, significant differences in methodology that may account for differences in signaling pathways activated. Aragon *et al.* (2016), utilized an isolated *ex vivo* wire myographic preparation of mouse aorta segments. This is a well-established and useful tool for explorations of vascular function, but this technique differs in several important ways from our work. In the present study, the use of an *in vivo* preparation allowed for the examination of vessels as they actively function, not removed from neural, mechanical, and humoral inputs and without pre-constriction. Second, the aorta fundamentally differs in form and function from the resistance vasculature, and disparate vascular segments often exhibit different functional responses to the same stimuli (Abukabda *et al.*, 2016, 2017), thus direct comparisons made between these 2 studies are limited. To reconcile our findings with those of Aragon *et al.*, it will be necessary to perform similar *in vivo* intravital investigation of the arterioles of CD36 KO mice following MWCNT exposure. Indeed, future research is warranted to determine the relative contributions of CD47 versus CD36, as well as which downstream targets are predominantly responsible for microvascular dysfunction.

Acute single exposure to MWCNT has been associated with pulmonary inflammation at the 24-h timepoint as assessed by bronchoalveolar lavage (BAL) (ie, polymorphonucleocyte count, albumin, lactate dehydrogenase content) (Porter *et al.*, 2010). Some studies have found that BAL fluid and macrophages have elevated inflammatory cytokines (including TNFα, IL-6, IL-1α, and IL-1β), as well as other markers of inflammation, such as lactate dehydrogenase, mucin, and surfactant protein-D (SP-D) at day 1 postMWCNT exposure (Dong *et al.*, 2015; Han *et al.*, 2010). IL1-β and IL-18 secretion has also been shown to be stimulated by exposure to raw or functionalized MWCNT in cultured macrophages (Hamilton *et al.*, 2013). In this study, we saw no significant difference tissue or circulating cytokines between MWCNT and sham exposed WT groups. Other studies have also shown no changes in cytokine production following MWCNT exposure. Mitchell et al. observed no inflammation or changes in lung mRNA IL-10 or IL-6 at 24 h following MWCNT exposure (Mitchell *et al.*, 2007). Elgrabli *et al.* observed that no changes in BAL mRNA in the lung for IL-1β, IL-6, IFNγ, COX2, and iNOS or protein levels for IL-1α, IL-1β, IL-2, IL-4, IL-6, IFNγ, TNFα from 1 to 180 days postMWCNT exposure (Elgrabli *et al.*, 2008). At present, it is not clear why there are divergent responses, but most likely is due to differences in the methodology approaches and potentially the exposure paradigm. We did, however, observe changes in several cytokines in our CD47 KO animals following MWCNT exposure (Figure 5). CD47 engagement can limit cytokine secretion (Demeure *et al.*, 2000), while CD47 blocking in macrophages has the opposite effect (Weiskopf *et al.*, 2015). It is

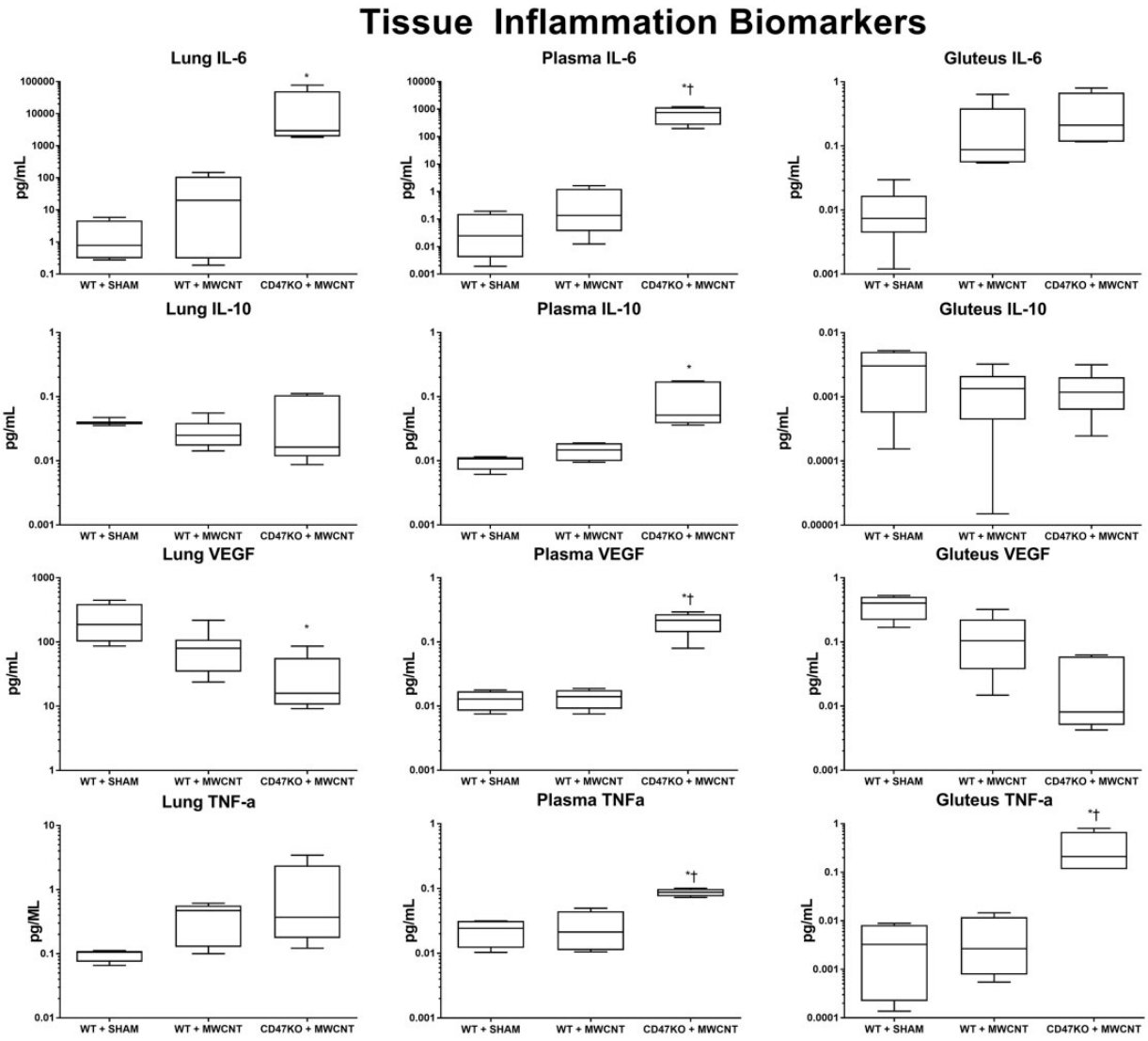

Figure 5. Tissue inflammation biomarkers. Asterisk indicates difference from WT + SHAM group ($p < .05$). Dagger indicates difference from WT + MWCNT ($p < .05$). No differences were observed between groups in measured levels of or IL-1 Number of animals studied: WT + SHAM ($n = 14$), WT + MWCNT ($n = 5$), CD47 KO + MWCNT ($n = 6$).

possible that the cytokine changes observed are simply due to this effect, and not a result of MWCNT exposure. Our results, combined with those from other studies, allow us to make inferences about the role of the measured cytokines and their potential involvement in mediating peripheral endothelial dysfunction. The fact that in WT + MWCNT we observed no changes in cytokines in any tissues, but observed substantial inhibitions of vasodilation and increases in leukocyte adhesion, while in the CD47 KO + MWCNT group the opposite was true, suggests that either the observational window for these animals was missed, or these cytokines are not playing a significant role in mediating the observed microvascular dysfunction.

Several important limitations should be noted about this work. First, only a single particle, dose, and time-point were examined and, as such, inferences about the role of TSP-1/CD47 following exposure to other particulate matter, at other doses, or at time points other than 24 h postexposure are only speculative. Second, while we expect that the microvascular response in the skeletal muscle to be generally representative of systemic responses, variations in reactivity, receptor density, and hemodynamics mean that our observations may only be relevant to the studied vascular bed: skeletal muscle. Future work should investigate the role of TSP-1/CD47 in microvascular function in other tissues, such as liver, kidneys, retina, etc.

In summary, 24 h following pulmonary exposure to MWCNT, CD47 KO animals exhibited no loss of vasodilatory function and no change in leukocyte-endothelial interaction that is found in WT animals. No alterations in blood ROS status were observed, however MWCNT exposure lowered lung and plasma NOx in WT animals while CD47 KO were unaffected. Inflammatory cytokines were unchanged in WT animals following exposure, while a significant shift in pro-inflammatory factors was observed in CD47 KO animals. These data complement earlier findings that microvascular dysfunction following MWCNT is TSP-1 dependent, and indicate that TSP-1/CD47 axis is an important mediator involved in the vascular dysfunction associated with MWCNT exposure.

Given that TSP-1/CD47 signaling has been shown to be activated in other disease states, including pulmonary arterial hypertension (Bauer *et al.*, 2012), peripheral and coronary artery disease (Choi *et al.*, 2012; Smadja *et al.*, 2011), and inclusion body myositis (Salajegheh *et al.*, 2007), it is reasonable to speculate

that ENM exposures may generate or exacerbate preexisting diseases in which the common denominator is vascular endothelial dysfunction. Therapeutic interventions aimed at the TSP-1/CD47 axis may help to reduce microvascular dysfunction not only in response to ENM exposure, but potentially other conditions that involve inhibition or reduced NO bioavailability.

ACKNOWLEDGEMENTS

The authors would like to thank Carroll McBride and Michael Wolfarth for their expert technical assistance.

FUNDING

National Institutes of Health (R01-ES015022 to T.R.N., 3P01AG043376-02S1 and 5P20GM109098 to E.E.K.); and the National Science Foundation Cooperative Agreement (1003907 to T.R.N., DGE-1144676 to W.K.M.).

REFERENCES

Abukabda, A. B., Stapleton, P. A., McBride, C. R., Yi, J., and Nurkiewicz, T. R. (2017). Heterogeneous vascular bed responses to pulmonary titanium dioxide nanoparticle exposure. *Front. Cardiovasc. Med.* **4**, 33.

Abukabda, A. B., Stapleton, P. A., and Nurkiewicz, T. R. (2016). Metal nanomaterial toxicity variations within the vascular system. *Curr. Environ. Health Rep.* **3**, 379–391.

Aragon, M., Erdely, A., Bishop, L., Salmen, R., Weaver, J., Liu, J., Hall, P., Eye, T., Kodali, V., and Zeidler-Erdely, P. (2016). MMP-9-dependent serum-borne bioactivity caused by multiwalled carbon nanotube exposure induces vascular dysfunction via the CD36 scavenger receptor. *Toxicol. Sci.* **150**, 488–498.

Aragon, M. J., Topper, L., Tyler, C. R., Sanchez, B., Zychowski, K., Young, T., Herbert, G., Hall, P., Erdely, A., Eye, T., *et al.* (2017). Serum-borne bioactivity caused by pulmonary multiwalled carbon nanotubes induces neuroinflammation via blood–brain barrier impairment. *Proc. Natl. Acad. Sci. U.S.A.* **114**, E1968.

Azcutia, V., Stefanidakis, M., Tsuboi, N., Mayadas, T., Croce, K. J., Fukuda, D., Aikawa, M., Newton, G., and Luscinskas, F. W. (2012). Endothelial CD47 promotes vascular endothelial-cadherin tyrosine phosphorylation and participates in T cell recruitment at sites of inflammation in vivo. *J. Immunol.* **189**, 2553–2562.

Baenzige, N. L., Brodie, G. N., and Majerus, P. W. (1971). Thrombin-sensitive protein of human platelet membranes. *Proc. Natl. Acad. Sci. U.S.A.* **68**, 240.

Bakand, S., Hayes, A., and Dechsakulthorn, F. (2012). Nanoparticles: A review of particle toxicology following inhalation exposure. *Inhal. Toxicol.* **24**, 125–135. (Review).

Barclay, A. N. (2009). Signal regulatory protein alpha (SIRPα)/CD47 interaction and function. *Curr. Opin. Immunol.* **21**, 47–52.

Bauer, E. M., Qin, Y., Miller, T. W., Bandle, R. W., Csanyi, G., Pagano, P. J., Bauer, P. M., Schnermann, J., Roberts, D. D., and Isenberg, J. S. (2010). Thrombospondin-1 supports blood pressure by limiting eNOS activation and endothelial-dependent vasorelaxation. *Cardiovasc. Res.* **88**, 471–481.

Bauer, P. M., Bauer, E. M., Rogers, N. M., Yao, M. Y., Feijoo-Cuaresma, M., Pilewski, J. M., Champion, H. C., Zuckerbraun, B. S., Calzada, M. J., and Isenberg, J. S. (2012). Activated CD47 promotes pulmonary arterial hypertension through targeting caveolin-1. *Cardiovasc. Res.* **93**, 682–693.

Bonetti, P. O., Lerman, L. O., and Lerman, A. (2003). Endothelial dysfunction—A marker of atherosclerotic risk. *Arterioscler. Thromb. Vasc. Biol.* **23**, 168–175.

Bonner, J. C., Silva, R. M., Taylor, A. J., Brown, J. M., Hilderbrand, S. C., Castranova, V., Porter, D., Elder, A., Oberdorster, G., Harkema, J. R., *et al.* (2013). Interlaboratory evaluation of rodent pulmonary responses to engineered nanomaterials: The NIEHS Nano GO Consortium. *Environ. Health Perspect.* **121**, 676–682.

Braman, R. S., and Hendrix, S. A. (1989). Nanogram nitrite and nitrate determination in environmental and biological materials by vanadium(III) reduction with chemiluminescence detection. *Anal. Chem.* **61**, 2715–2718.

Brevetti, G., Schiano, V., and Chiariello, M. (2008). Endothelial dysfunction: A key to the pathophysiology and natural history of peripheral arterial disease? *Atherosclerosis* **197**, 1–11.

Cao, Y., Jacobsen, N. R., Danielsen, P. H., Lenz, A. G., Stoeger, T., Loft, S., Wallin, H., Roursgaard, M., Mikkelsen, L., and Moller, P. (2014). Vascular effects of multiwalled carbon nanotubes in dyslipidemic ApoE(/) mice and cultured endothelial cells. *Toxicol. Sci.* **138**, 104–116.

Choi, K. Y., Kim, D. B., Kim, M. J., Kwon, B. J., Chang, S. Y., Jang, S. W., Cho, E. J., Rho, T. H., and Kim, J. H. (2012). Higher plasma thrombospondin-1 levels in patients with coronary artery disease and diabetes mellitus. *Korean Circ. J.* **42**, 100–106.

Csanyi, G., Yao, M., Rodriguez, A. I., Ghouleh, I. A., Sharifi-Sanjani, M., Frazziano, G., Huang, X., Kelley, E. E., Isenberg, J. S., and Pagano, P. J. (2012). Thrombospondin-1 regulates blood flow via CD47 receptor mediated activation of NADPH oxidase 1. *Arterioscler. Thromb. Vasc. Biol.* **32**, 2966.

Davignon, J., and Ganz, P. (2004). Role of endothelial dysfunction in atherosclerosis. *Circulation* **109**, III27–III32.

Deem, T. L., and Cook-Mills, J. M. (2004). Vascular cell adhesion molecule 1 (VCAM-1) activation of endothelial cell matrix metalloproteinases: Role of reactive oxygen species. *Blood* **104**, 2385–2393.

DelMaschio, A., Zanetti, A., Corada, M., Rival, Y., Ruco, L., Lampugnani, M. G., and Dejana, E. (1996). Polymorphonuclear leukocyte adhesion triggers the disorganization of endothelial cell-to-cell adherens junctions. *J. Cell Biol.* **135**, 497–510.

Demeure, C. E., Tanaka, H., Mateo, V., Rubio, M., Delespesse, G., and Sarfati, M. (2000). CD47 engagement inhibits cytokine production and maturation of human dendritic cells. *J. Immunol.* **164**, 2193–2199.

Dong, J., Porter, D. W., Batteli, L. A., Wolfarth, M. G., Richardson, D. L., and Ma, Q. (2015). Pathologic and molecular profiling of rapid-onset fibrosis and inflammation induced by multiwalled carbon nanotubes. *Arch. Toxicol.* **89**, 621–633.

Elgrabli, D., Abella-Gallart, S., Robidel, F., Rogerieux, F., Boczkowski, J., and Lacroix, G. (2008). Induction of apoptosis and absence of inflammation in rat lung after intratracheal instillation of multiwalled carbon nanotubes. *Toxicology* **253**, 131–136.

Flurkey, K., Currer, J., and Harrison, D. (2007). The mouse in aging research. In The Mouse in Biomedical Research, 2nd ed. (M. T. Davisson, F. W. Quimby, S. W. Barthold, C. E. Newcomer, and A. L. Smith, Eds.) pp. 637-672. Burlington: Academic Press.

Granger, D. N., and Senchenkova, E. (2010). Leukocyte–endothelial cell adhesion. In *Inflammation and the Microcirculation*, pp. 29-40. Morgan & Claypool Life Sciences, San Rafael, CA.

Hamilton, R. F., Xiang, C. C., Li, M., Ka, I., Yang, F., Ma, D. L., Porter, D. W., Wu, N. Q., and Holian, A. (2013). Purification and sidewall functionalization of multiwalled carbon

nanotubes and resulting bioactivity in two macrophage models. *Inhal. Toxicol.* **25**, 199–210.

Han, J. H., Lee, E. J., Lee, J. H., So, K. P., Lee, Y. H., Bae, G. N., Lee, S. B., Ji, J. H., Cho, M. H., and Yu, I. J. (2008). Monitoring multiwalled carbon nanotube exposure in carbon nanotube research facility. *Inhal. Toxicol.* **20**, 741–749.

Han, S. G. (2016). Effects of multi-walled carbon nanotubes in the lungs and aortas of ApoE-deficient mice fed a normal diet. *J. Nanosci. Nanotechnol.* **16**, 8019–8024. Article).

Han, S. G., Andrews, R., and Gairola, C. G. (2010). Acute pulmonary response of mice to multi-wall carbon nanotubes. *Inhal. Toxicol.* **22**, 340–347.

Heitzer, T., Schlinzig, T., Krohn, K., Meinertz, T., and Munzel, T. (2001). Endothelial dysfunction, oxidative stress, and risk of cardiovascular events in patients with coronary artery disease. *Circulation* **104**, 2673–2678.

Hopps, E., Lo Presti, R., and Caimi, G. (2009). Pathophysiology of polymorphonuclear leukocyte in arterial hypertension. *Clin. Hemorheol. Microcirc.* **41**, 209–218. Review).

Inoue, K., Koike, E., Yanagisaw, R., Hirano, S., Nishikawa, M., and Takano, H. (2009). Effects of multi-walled carbon nanotubes on a murine allergic airway inflammation model. *Toxicol. Appl. Pharmacol.* **237**, 306–316.

Isenberg, J. S., Ridnour, L. A., Perruccio, E. M., Espey, M. G., Wink, D. A., and Roberts, D. D. (2005). Thrombospondin-1 inhibits endothelial cell responses to nitric oxide in a cGMP-dependent manner. *Proc. Natl. Acad. Sci. U.S.A.* **102**, 13141.

Isenberg, J. S., Wink, D. A., and Roberts, D. D. (2006). Thrombospondin-1 antagonizes nitric oxide-stimulated vascular smooth muscle cell responses. *Cardiovasc. Res.* **71**, 785–793.

Kar, S., and Kavdia, M. (2012). Local oxidative and nitrosative stress increases in the microcirculation during leukocytes-endothelial cell interactions. *PLoS One* **7**, e38912.

Knuckles, T. L., Stapleton, P. A., Minarchick, V. C., Esch, L., McCawley, M., Hendryx, M., and Nurkiewicz, T. R. (2013). Air pollution particulate matter collected from an Appalachian mountaintop mining site induces microvascular dysfunction. *Microcirculation* **20**, 158–169.

Lagadec, P., Dejoux, O., Ticchioni, M., Cottrez, F., Johansen, M., Brown, E. J., and Bernard, A. (2003). Involvement of a CD47-dependent pathway in platelet adhesion on inflamed vascular endothelium under flow. *Blood* **101**, 4836–4843.

LeBlanc, A. J., Cumpston, J. L., Chen, B. T., Frazer, D., Castranova, V., and Nurkiewicz, T. R. (2009). Nanoparticle inhalation impairs endothelium-dependent vasodilation in subepicardial arterioles. *J. Toxicol. Environ. Health A* **72**, 1576–1584.

LeBlanc, A. J., Moseley, A. M., Chen, B. T., Frazer, D., Castranova, V., and Nurkiewicz, T. R. (2010). Nanoparticle inhalation impairs coronary microvascular reactivity via a local reactive oxygen species-dependent mechanism. *Cardiovasc. Toxicol.* **10**, 27–36.

Mandler, W. K., Nurkiewicz, T. R., Porter, D. W., and Olfert, I. M. (2017). Thrombospondin-1 mediates multi-walled carbon nanotube induced impairment of arteriolar dilation. *Nanotoxicology* **11**, 112–122.

Mercer, R. R., Hubbs, A. F., Scabilloni, J. F., Wang, L., Battelli, L. A., Schwegler-Berry, D., Castranova, V., and Porter, D. W. (2010). Distribution and persistence of pleural penetrations by multi-walled carbon nanotubes. *Part Fibre Toxicol.* **7**, 28.

Mercer, R. R., Hubbs, A. F., Scabilloni, J. F., Wang, L. Y., Battelli, L. A., Friend, S., Castranova, V., and Porter, D. W. (2011). Pulmonary fibrotic response to aspiration of multi-walled carbon nanotubes. *Particle Fibre Toxicol.* **8**, 21.

Mercer, R. R., Scabilloni, J. F., Hubbs, A. F., Battelli, L. A., McKinney, W., Friend, S., Wolfarth, M. G., Andrew, M., Castranova, V., and Porter, D. W. (2013a). Distribution and fibrotic response following inhalation exposure to multi-walled carbon nanotubes. *Part Fibre Toxicol.* **10**, 33.

Mercer, R. R., Scabilloni, J. F., Hubbs, A. F., Wang, L., Battelli, L. A., McKinney, W., Castranova, V., and Porter, D. W. (2013b). Extrapulmonary transport of MWCNT following inhalation exposure. *Part Fibre Toxicol.* **10**, 38.

Mitchell, L. A., Gao, J., Wal, R. V., Gigliotti, A., Burchiel, S. W., and McDonald, J. D. (2007). Pulmonary and systemic immune response to inhaled multiwalled carbon nanotubes. *Toxicol. Sci.* **100**, 203–214. (Article).

Narizhneva, N. V., Razorenova, O. V., Podrez, E. A., Chen, J. H., Chandrasekharan, U. M., DiCorleto, P. E., Plow, E. F., Topol, E. J., and Byzova, T. V. (2005). Thrombospondin-1 up-regulates expression of cell adhesion molecules and promotes monocyte binding to endothelium. *FASEB J.* **19**, 1158.

Nurkiewicz, T. R., Porter, D. W., Hubbs, A. F., Stone, S., Chen, B. T., Frazer, D. G., Boegehold, M. A., and Castranova, V. (2009). Pulmonary nanoparticle exposure disrupts systemic microvascular nitric oxide signaling. *Toxicol. Sci.* **110**, 191–203.

Perticone, F., Ceravolo, R., Pujia, A., Ventura, G., Iacopino, S., Scozzafava, A., Ferraro, A., Chello, M., Mastroroberto, P., Verdecchia, P., *et al.* (2001). Prognostic significance of endothelial dysfunction in hypertensive patients. *Circulation* **104**, 191–196.

Petrak, O., Widimsky, J., Jr, Zelinka, T., Kvasnicka, J., Strauch, B., Holaj, R., Stulc, T., Kvasnicka, T., Bilkova, J., and Skrha, J. (2006). Biochemical markers of endothelial dysfunction in patients with endocrine and essential hypertension. *Physiol. Res.* **55**, 597–602.

Porter, D., Sriram, K., Wolfarth, M., Jefferson, A., Schwegler-Berry, D., Andrew, M., and Castranova, V. (2008). A biocompatible medium for nanoparticle dispersion. *Nanotoxicology* **2**, 144–154.

Porter, D. W., Hubbs, A. F., Chen, B. T., McKinney, W., Mercer, R. R., Wolfarth, M. G., Battelli, L., Wu, N., Sriram, K., Leonard, S., *et al.* (2012). Acute pulmonary dose-responses to inhaled multi-walled carbon nanotubes. *Nanotoxicology* **7**, 1179–1194.

Porter, D. W., Hubbs, A. F., Mercer, R. R., Wu, N., Wolfarth, M. G., Sriram, K., Leonard, S., Battelli, L., Schwegler-Berry, D., and Friend, S. (2010). Mouse pulmonary dose- and time course-responses induced by exposure to multi-walled carbon nanotubes. *Toxicology* **269**, 136–147.

Salajegheh, M., Raju, R., Schmidt, J., and Dalakas, M. C. (2007). Upregulation of thrombospondin-1(TSP-1) and its binding partners, CD36 and CD47, in sporadic inclusion body myositis. *J. Neuroimmunol.* **187**, 166–174. (Article).

Shvedova, A. A., Kisin, E., Murray, A. R., Johnson, V. J., Gorelik, O., Arepalli, S., Hubbs, A. F., Mercer, R. R., Keohavong, P., Sussman, N., *et al.* (2008). Inhalation vs. aspiration of single-walled carbon nanotubes in C57BL/6 mice: Inflammation, fibrosis, oxidative stress, and mutagenesis. *Am. J. Physiol. Lung Cell. Mol. Physiol.* **295**, L552–L565.

Sitia, S., Tomasoni, L., Atzeni, F., Ambrosio, G., Cordiano, C., Catapano, A., Tramontana, S., Perticone, F., Naccarato, P., Camici, P., *et al.* (2010). From endothelial dysfunction to atherosclerosis. *Autoimmun. Rev.* **9**, 830–834.

Smadja, D. M., d'Audigier, C., Bieche, I., Evrard, S., Mauge, L., Dias, J. V., Labreuche, J., Laurendeau, I., Marsac, B., Dizier, B., *et al.* (2011). Thrombospondin-1 is a plasmatic marker of peripheral arterial disease that modulates endothelial

progenitor cell angiogenic properties. *Arterioscler. Thromb. Vasc. Biol.* **31**, 551–559. (Article).

Stapleton, P. A., Minarchick, V. C., Cumpston, A. M., McKinney, W., Chen, B. T., Sager, T. M., Frazer, D. G., Mercer, R. R., Scabilloni, J., Andrew, M. E., *et al.* (2012). Impairment of coronary arteriolar endothelium-dependent dilation after multi-walled carbon nanotube inhalation: A time-course study. *Int. J. Mol. Sci.* **13**, 13781–13803.

Thompson, L. C., Frasier, C. R., Sloan, R. C., Mann, E. E., Harrison, B. S., Brown, J. M., Brown, D. A., and Wingard, C. J. (2014). Pulmonary instillation of multi-walled carbon nanotubes promotes coronary vasoconstriction and exacerbates injury in isolated hearts. *Nanotoxicology* **8**, 38–49.

Weiskopf, K., Ring, A., Garcia, K. C., and Weissman, I. (2015). CD47-blocking therapies stimulate macrophage cytokine secretion and are effective in a model of peritoneal carcinomatosis. *J. Immunother. Cancer* **3**, P248.

Zarbock, A., and Ley, K. (2009). The role of platelets in acute lung injury (ALI). *Front. Biosci.* **14**, 150–158.